Materials Today Bio 29 (2024) 101265

Contents lists available at ScienceDirect

Materials Today Bio

journal homepage: www.journals.elsevier.com/materials-today-bio

Photo-crosslinking injectable Photothermal antibacterial hydrogel based on quaternary ammonium grafted chitosan and hyaluronic acid for infected wound healing

Xinbo Ma [a,1], Aoao Wang [b,1], Xuelian Zhang [c,1], Juan Zhang [d,1], Jiawei Li [a], Xi Fu [e], Peng Wang [f,**], Yantao Zhao [b,***], Xiaonan Huang [a,*]

[a] Department of Chemistry, Capital Normal University, No. 105 West 3rd Ring North Rd, Beijing 100048, China
[b] Senior Department of Orthopaedics, The Fourth Medical Center of PLA General Hospital, Beijing, China
[c] Department of Endocrinology, China-Japan Friendship Hospital, 2 Yinghua East Road, Chaoyang District,Beijing 100029, China
[d] Bio-manufacturing and Rapid Prototyping Technology Key Laboratory Dept.of Mechanical Engineering, Tsinghua University, Beijing, China
[e] Sichun Jianzhu Hospital, No.9 Xinghui East Road, Jinniu District, Chengdu City, Sichuan Province, China
[f] Department of Neurosurgery, The First Medical Center of Chinese PLA General Hospital, 28 Fuxing Road, Beijing,100853, China

ARTICLE INFO

Keywords:
Injectable
Photo-crosslinking hydrogel
Photothermal
Antibacterial
Infected wound healing

ABSTRACT

Antibacterial hydrogels not only provide a better environment for skin wounds to avoid infection but also accelerate wound healing. Herein, chitosan modified by a quaternary ammonium salt (CQ), and hyaluronic acid grafted with methacrylate (HM) were designed and synthesized to prepare an injectable photo-crosslinking hydrogel for wound dressing with inherent antibacterial and photothermal properties. CQ and HM exhibited excellent biocompatibility, improved water retention, and antibacterial activity, illustrating vast potential as an antibacterial material in various applications. MXene, a type of 2D nanomaterial, has been widely researched due to its photothermal properties. The CQ and HM polymer precursor could be mixed with Mxene and then crosslinked with 395 nm UV radiation under mild conditions to form a 3D network structure CQ-HM/MXene hydrogel. This hydrogel displayed an appropriate swelling ratio, elastic modulus, photothermal property and excellent biocompatibility. The injectable property of the hydrogel allowed it to easily cover the wound. In vitro and in vivo studies showed that the injectable hydrogel had low cytotoxicity and excellent antibacterial properties, which could help promote wound healing. In summary, this novel CQ-HA/MXene hydrogel has the potential for application in skin wound healing due to inherent antibacterial activity and photothermal effect.

1. Introduction

As the body's largest organ, the skin plays a crucial role in regulating body temperature, protecting against pathogens, and performing metabolic and immune functions [1]. However, various factors such as physiological abnormalities, as well as mechanical, thermal, or physical stressors, can lead to skin damage [2,3]. In particular, bacterial infections often result in significant tissue damage, prolonged inflammatory responses, and delayed wound healing [4]. The disruption or deterioration of skin tissues and organ structures caused by bacterial infections can lead to decreased skin perfusion and heightened inflammation, thereby hampering the natural healing process of the wound. The restoration of skin integrity, homeostasis, and protective function post-injury is crucial for most organisms. In clinical practice, antibiotics are commonly used to prevent and treat wound infections [5]. Nevertheless, the excessive use of antibiotics has given rise to the development of multidrug-resistant bacterial strains, leading to the persistence of chronic wounds. As a result, the rapid treatment of highly infectious and

* Corresponding author.
** Corresponding author.
*** Corresponding author.
E-mail addresses: 1653299104@qq.com (X. Ma), Waa1060656551@163.com (A. Wang), zhangxuelian@zryhyy.com.cn (X. Zhang), zhang_juan@mail.tsinghua.edu.cn (J. Zhang), 1349331612@qq.com (J. Li), 15882325081@139.com (X. Fu), userzyt@qq.com (P. Wang), wangpeng301@foxmail.com (Y. Zhao), huangxn@cnu.edu.cn (X. Huang).
[1] These authors have contributed equally to this work and share first authorship.

https://doi.org/10.1016/j.mtbio.2024.101265
Received 10 June 2024; Received in revised form 9 September 2024; Accepted 22 September 2024
Available online 23 September 2024

chronic wounds poses a significant global challenge. Traditional clinical approaches to skin injuries involve the use of wound dressings such as bandages, gauze, and lint. However, these conventional wound dressings face challenges during removal and may contribute to drug resistance. Hence, there is a pressing need to innovate and develop novel wound dressings for the treatment of non-healing chronic wounds [6,7] (In this study, we designed a photo-crosslinked hydrogel prepared by mixing modified chitosan, hyaluronic acid, and MXene, which is injectable and has photothermal properties (CQ-HA/MXene). It integrates excellent antibacterial performance and promotes re-epithelialization to accelerate the closure of infected wounds in rats (see Scheme 1).).

Biopolymers offer great promise in wound healing as they have the potential to modulate the wound-repair process [8]. Hydrogels prepared with biopolymers stand out as a leading candidate for wound healing due to their tunable physical and mechanical properties which could be used to mimic the native extracellular matrix and provide protection to wounds [9,10]. For instance, hyaluronic acid (HA), a glycosaminogly based polymer, can be found in the extracellular matrix, is a crucial component of tissue in vertebrates [11]. Its unique physicochemical properties, such as biodegradability and biocompatibility, play a key role in influencing cell behavior such as differentiation, proliferation, and migration during tissue development and regeneration processes [12]. Therefore, HA has the potential to be developed as a regenerative biomaterial for treating skin lesions and injuries [13]. Chitin, a natural material derived from fungi, crustaceans, and insects, has been widely recognized for its eco-friendly properties. When chitin undergoes deacetylation, it transforms into chitosan (CS), a biocompatible, biodegradable, and non-toxic substance with remarkable biological activity [10,11]. As a cationic polymer, chitosan can interact with negatively charged biomolecules due to its unique composition, sequence, and chain length. Simultaneously, to enhance its versatility, chitosan can be chemically modified to create derivatives. The superior biocompatibility and antibacterial properties have made CS a valuable material in tissue engineering. Additionally, chitosan's antimicrobial and wound-healing properties, as well as its cholesterol-binding capability, have led to its use in various products. Its potential in drug delivery, tissue engineering, and water treatment underscores the importance of chitosan in both scientific research and industrial applications [14,15].

Thermal assisted wound dressings have been investigated for their potential in promoting wound healing [15,16]. Heat-radiating dressings have been studied as a way to enhance skin wound healing by stimulating increased capillary perfusion. By applying topical radiant heating to wounds and raising the temperature, it has been observed that dermal blood flow and lymphocyte extravasation are increased [17]. The findings suggest that incorporating thermal radiation adjuncts can significantly accelerate the rate of wound healing [18]. MXene, a novel class of two-dimensional (2D) nanomaterials, comparable to graphene, exhibits exceptional mechanical strength and a significant specific surface area [19–21]. MXenes' remarkable capacity for near-infrared (NIR) light absorption can transfer the light energy to heat, which induces its excellent photothermal conversion capabilities. These properties of MXenes demonstrate their potential application for biomedical therapy through the phenomenon known as the photothermal transfer effect. Compared with other inorganic nanomaterials, MXene has shown showed photothermal ability with near-infrared region I (NIR-I) excitation light, demonstrating its ability to effectively penetrate infected tissues [22]. Simutaneously, after being modified with other metals or compounds, the Mxene can also illustrate enzyme-like activity with chemodynamic therapy (CDT) and peroxidase (POD)-like activity [23,24].

In this study, a novel injectable photo-crosslinked antibacterial hydrogel with photothermal properties was developed by combining CS, hyaluronic acid, and MXene. The hyaluronic acid was modified with methacrylic anhydride to form hyaluronic acid-methacrylate (HM), which could be photo-crosslinked to form hydrogel. CS was modified with 3-chloro-2-hydroxypropyl trimethyl ammonium chloride to form CS-quaternary ammonium salt (CQ), which enhanced the inherent

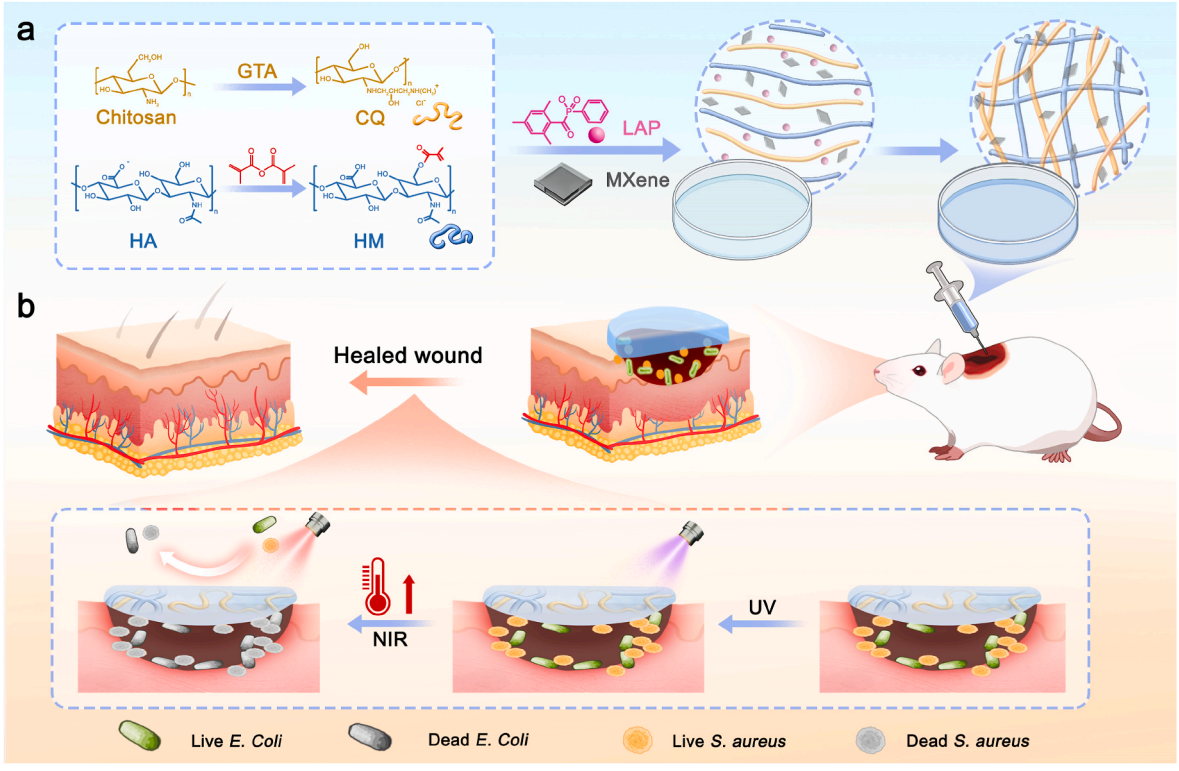

Scheme 1. (a) Schematic illustrations of the synthesis of injectable photothermal CQ-HM/MXene hydrogels; (b)The mechanism of infected wound healing treated with the photothermal CQ-HM/MXene hydrogel with antibacterial properties.

antibacterial properties of the polymer. MXene was incorporated into the HM and CQ solution, and the mixture precursor was injected onto the wound site and crosslinked using 395 nm UV light radiation in the presence of the photoinitiator lithium acylphospinate (LAP) to form the CQ-HM/MXene hydrogel. The resulting injectable photo-crosslinked CQ-HM/MXene hydrogel demonstrated excellent biocompatibility, water retention, swelling capacity. Furthermore, the hydrogel also demonstrated excellent photothermal properties. The combination of CQ's intrinsic antibacterial properties and MXene's photothermal effects resulted in the CQ-HM/MXene hydrogel, which could exhibit enhanced antibacterial efficacy and accelerate the healing of infected wounds. These findings indicated that this innovative hydrogel has considerable promise for clinical applications in the treatment of infectious wounds.

2. Results

2.1. Synthesis and characterization of CQ-HM/MXene hydrogel

To meet the requirements for photothermal therapy in wound healing, a biodegradable in situ injectable photo-crosslinked antibacterial hydrogel was prepared using hyaluronic acid and CS modified with methylacrylate and quaternary ammonium salt respectively. Methylarylate could be crosslinked by free radicals to form the 3D network structure of the hydrogel, and quaternary ammonium salt could enhance the antibacterial properties of CS [25–27].

First, hyaluronic acid was grafted with methylacrylate to form HM (Fig. 1(a)). Fig. 1(b) and (c) displayed the ^{1}H NMR and FTIR spectra of HM. The peak at δ 3–4 ppm was the characteristic peak of hydrogen in the glucose cyclic structure on the backbone of the HM. The peak at δ 1.86 ppm was the characteristic peak of methyl group of methylacrylate on HM, and the peak at δ 2.03 ppm was the characteristic peak of methyl on the side chain N-acetylglucosamine. Consequently, peaks at δ 5.51 ppm and δ 5.98 ppm were the characteristic peaks corresponding to the hydrogen in the double bond region of the MA group, which indicating that the successful modification of the methylarylate on the HA and comparing the integral of the proton characteristic peak in the double bond of the MA, the grafting ratio was calculated to be 16 %. Simultaneously, the modification did not disrupt the primary structure of HA.

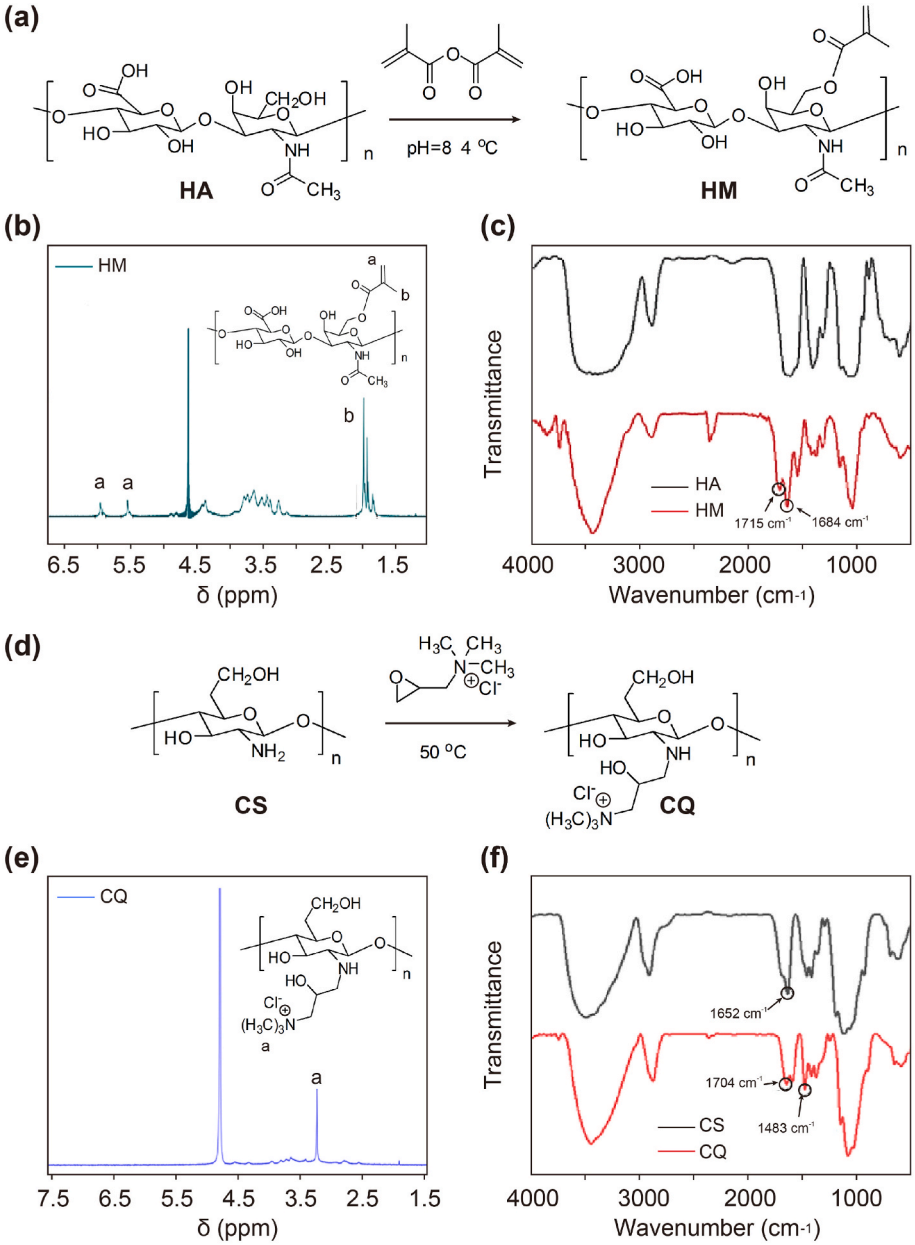

Fig. 1. Scheme for the synthesis of HM (a) and CQ (d); (b) ~ (c) ^{1}H NMR and FTIR characterization of HM; (e) ~ (f) ^{1}H NMR and FTIR characterization of CQ.

Consequently, FTIR spectra of HM showed the stretching vibration peak of C=O at 1715 cm^{-1} and C=C at 1650 cm^{-1} which also demonstrated the successfully grafting of the methylacrylate on the hyaluronic acid.

In order to increase the antibacterial properties of the hydrogel, chitosan was grafted with 3-chloro-2-hydroxypropyl trimethyl ammonium chloride to form CQ (Fig. 1(d)). Fig. 1(e) displayed the ^1H NMR of CQ. The degree of substitution of glycidyl trimethylammonium chloride grafted onto CQ can be calculated by comparing the integral of the proton characteristic peak in the trimethyl region at δ 2.73 ppm, giving a result of 26 % according to Refs. [28,29]. The FTIR spectra of CS and CQ were shown in Fig. 1(f). The broad band at around 3435 cm^{-1} could be attributed to the stretching vibration peaks of O−H and N-H of CQ. The stretching vibration peak of aliphatic C−H at 2870 cm^{-1} was assigned to the characteristic bands. In addition, the band at 1652 cm^{-1} was attributed to the in-plane bending vibration peak of secondary amine N−H on the CS. The peak of N−H on CQ shift to 1604 cm^{-1} was significantly weakened after the glycidyl trimethylammonium chloride with the amino group of the CS chain. All of the above results confirmed that the glycidyl trimethylammonium chloride groups have been successfully grafted onto the CS [30–32].

2.2. Characterization of CQ-HA/MXene hydrogel

To prepare the hydrogel, HM, CQ and Ti_3C_2 Mxene were mixed with the light initiator LAP. Upon expsure to 395 nm UV light, the methylacrylate was cross-linked by the radicals released by LAP, resulting in the formation of the hydrogel [33]. The prepared four groups of hydrogels were named CQ-HM, CQ-HM/MXene-1, CQ-HM/MXene-2, and CQ-HM/MXene-3 with different amounts of Mxene (0 mg/mL, 1 mg/mL, 2 mg/mL, 3 mg/mL). Consequently, the four groups of hydrogels were freeze-dried in a freeze-dryer at −80 °C. The lyophilized hydrogels were meticulously sliced and subjected to a 60 s gold spraying process and then characterized using scanning electron microscopy (SEM). Fig. 2 (a) illustrated the porous characteristics of the hydrogel surfaces. The CQ-HM, CQ-HM/MXene-1, CQ-HM/MXene-2, and CQ-HM/MXene-3 hydrogels exhibited larger pore sizes on their surfaces. The presence of MXene could result in a smoother surface texture with the MXene content increasing in the hydrogels. A specific region of the hydrogel was then selected for elemental analysis. Energy-dispersive X-ray spectroscopy (EDS) was performed to determine the elemental composition and visualize the distribution of elements within the hydrogel. Fig. 2 (b) displays the EDS analysis of the hydrogel results, which revealed that the titanium element exhibited a gradual increase with the escalating quantity of MXene, suggesting that MXene could be retained homogeneously within the hydrogel matrix.

2.3. Swelling analysis

The water absorption of the hydrogel was also evaluated through a swelling experiment. The CQ-HM, CQ-HM/MXene-1, CQ-HM/MXene-2, and CQ-HM/MXene-3 hydrogels previously prepared were sliced into cylindrical sheets of uniform volume and dimensions. The freeze-dried weight of each hydrogel was measured and denoted as W_0. Subsequently, the hydrogels were immersed in an equal volume of deionized

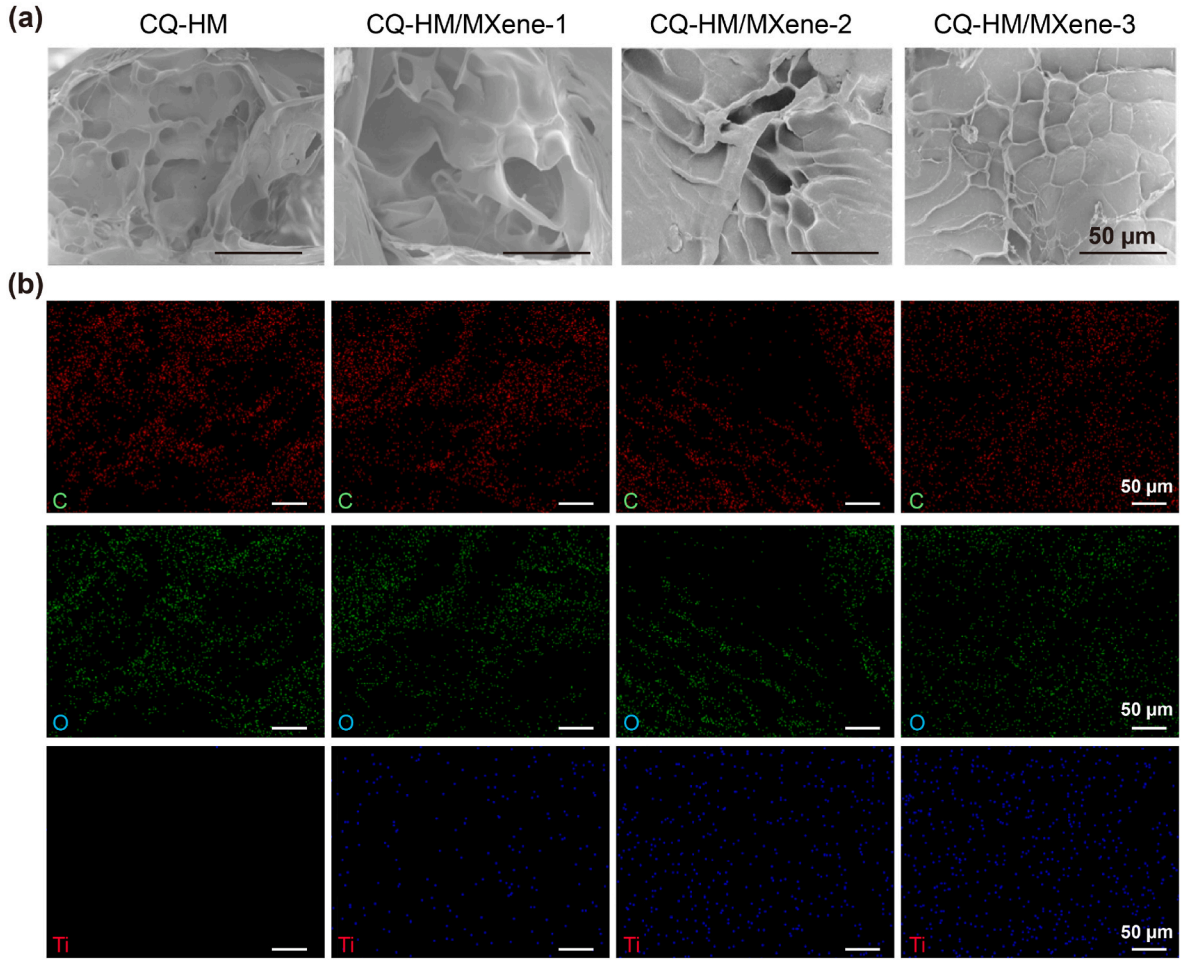

Fig. 2. (a) SEM image of hydrogels with different concentrations of MXene: CQ-HM, CQ-HM/MXene-1, CQ-HM/MXene-2, CQ-HM/MXene-3 hydrogels; (b) EDS-based elemental maps of CQ-HM, CQ-HM/MXene-1, CQ-HM/MXene-2, CQ-HM/MXene-3 hydrogels.

water at room temperature for 24 h. After removing the sample, any surface water was promptly dried with filter paper, and the weight was recorded as the swelling weight (W_t). The swelling ratio (W %) was calculated using the following equation:

$$W\% = \frac{W_t - W_0}{W_0} \times 100\%$$

Fig. 3 (a) illustrated the swelling ratio of hydrogels reaching 200 %, demonstrating that the excellent absorption properties of CQ-HM, CQ-HM/MXene-1, CQ-HM/MXene-2, and CQ-HM/MXene-3 hydrogels.

2.4. Rheological analysis

Subsequently, rheological properties of CQ-HA, CQ/HA-MXene-1, CQ/HA-MXene-2, and CQ/HA-MXene-3 hydrogels were detected using a Physical MCR rheometer. The rheology measurements were performed using a circular disk configuration, with the hydrogel positioned between parallel plates set at a precise 0.5 mm gap distance. Frequency and strain scanning were performed to analyze the storage modulus (G′) and loss modulus (G″), with real-time tracking of their changes throughout the measurement process. For oscillation frequency scanning, a 1 % strain amplitude was maintained once the hydrogel had stabilized. The angular frequency range was adjusted between 0.1 and 100 rad/s. During strain scanning, keep the frequency amplitude at 1 rad/s after the hydrogel has stabilized. Adjust the strain range between 0.1 and 200 %. In this context, an amplitude sweep was utilized to assess the storage modulus (G′) and the loss modulus (G″) within the linear viscoelastic region (Fig. 3 (b) and 3 (c)). Upon the establishment of the 3D crosslinked network structure, the CQ-HM, CQ-HM/MXene-1, CQ-HM/MXene-2, and CQ-HM/MXene-3 hydrogels exhibited elastic properties, characterized by a higher energy storage modulus G′ compared to the loss modulus G″, which showed almost no variation with stress and angular frequency models. The storage modulus G' of 1 kPa for CQ-HM, CQ-HM/MXene-1, CQ-HM/MXene-2, and CQ-HM/MXene-3 hydrogels demonstrated exceptional flexibility, enabling them to conform to the wound and mimic the properties of natural tissue matrix.

2.5. Photothermal properties

Photothermal therapy (PTT) utilizes an external light source to convert light energy into heat at the wound site, with the goal of eradicating pathogens. PTT emerges as a prominent alternative to traditional antibiotic treatments for infectious diseases, boasting high selectivity, minimal invasiveness, and negligible side effects [29,34]. Its non-invasive nature and low likelihood of inducing drug resistance further enhance its application potential as a therapeutic approach. CQ-HM, CQ-HM/MXene-1, CQ-HM/MXene-2, and CQ-HM/MXene-3 hydrogels were investigated by monitoring their temperature changes with 808 nm NIR irradiation. In order to assess the impact of different near-infrared (NIR) power levels on the photothermal characteristics, the CQ-HM/Mxene-1 hydrogel was selected to be irradiated by 808 nm NIR for 600 s using power settings of 0.5 W, 0.75 W, 1.0 W, 1.25 W, and 1.5 W with the light source positioned at a distance of 15 cm from the sample. Concurrently, real-time temperature fluctuations were recorded using an infrared imaging camera. The data demonstrated that the CQ-HM/MXene-1 hydrogel's temperature reached 54 °C under a light power of 1.5 W/cm^2, and 43 °C under a light power of 1.0 W/cm^2 for a duration of 600 s (Fig. 4(a) and (b)). Considering the potential harm to healthy skin from elevated temperatures, a power level of 1.0 W/cm^2 was chosen for subsequent photothermal experiments. In addition, the content of the MXene in the hydrogel was also measured to evaluate the best ratio of photothermal material in the hydrogel. The reported photothermal conversion efficiency of MXene as found to be 38.5 % [23]. CQ-HM, CQ-HM/MXene-1, CQ-HM/MXene-2, and CQ-HM/MXene-3 hydrogels with different MXene ratios were exposed to NIR at 808 nm for 600 s at a power of 1.0 W. Since no photothermal material MXene was added to the CQ-HM hydrogel, the application of NIR caused no obvious temperature changes. The temperature variations of the CQ-HM/MXene-3 hydrogel showed the highest contrast using an infrared thermograph and reached 49 °C (Fig. 4(c) and (d)). The temperature of CQ-HM/MXene-1, CQ-HM/MXene-2, and CQ-HM/MXene-3 increased by 13.5 °C, 15 °C, and 19 °C respectively. These results demonstrated that the CQ-HM/MXene hydrogels were capable of absorbing NIR energy and converting it into thermal energy, and that the higher the power and MXene content, the better the photothermal performance of the material. Furthermore, the reversibility of the photothermal effect of the hydrogel was assessed by conducting a cycle experiment involving NIR irradiation followed by natural cooling after turning off the laser. Fig. 4 (e) illustrated the temperature fluctuation of the CQ-HM/MXene-3 hydrogel during a single cycle. The cyclic process was repeated multiple times to evaluate the repeatability of the photothermal effect. In Fig. 4 (f), the temperature variation resulting from a four-cycle experiment of NIR irradiation and natural cooling is demonstrated. It is noteworthy that the photothermal effect of the sample remained consistent throughout the cycles. This can be attributed to the strong photothermal effect of MXene, which is effectively preserved within the hydrogel.

2.6. Cytotoxicity study

To assess the cytocompatibility and biological performance of the CQ-HM, CQ-HM/MXene-1, CQ-HM/MXene-2, and CQ-HM/MXene-3 hydrogels for potential biomedical applications, in vitro CCK (cell counting kit) and dead/live assays were conducted. These assays were performed. Using cells cultured in DMEM supplemented with 10 % bovine serum and 10 % DMSO. A cell suspension containing approximately 1 × 10^5 cells was inoculated onto 96-well cell culture plates and incubated in a 37 °C incubator with 5 % CO_2. After 24 h of incubation,

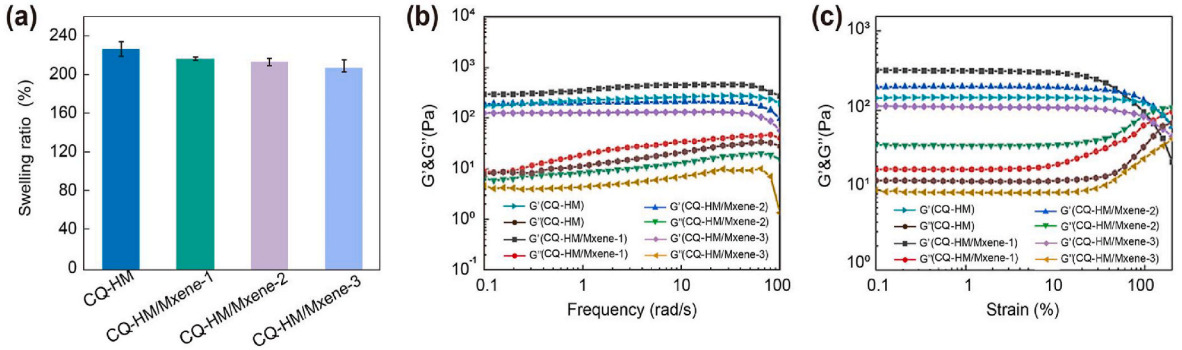

Fig. 3. (a) The swelling ratio of CQ-HM, CQ-HM/MXene-1, CQ-HM/MXene-2, and CQ-HM/MXene-3 hydrogels; (b) and (c) Rheological measurements of the CQ-HM, CQ-HM/MXene-1, CQ-HM/MXene-2, and CQ-HM/MXene-3 hydrogels with frequency and strain mode.

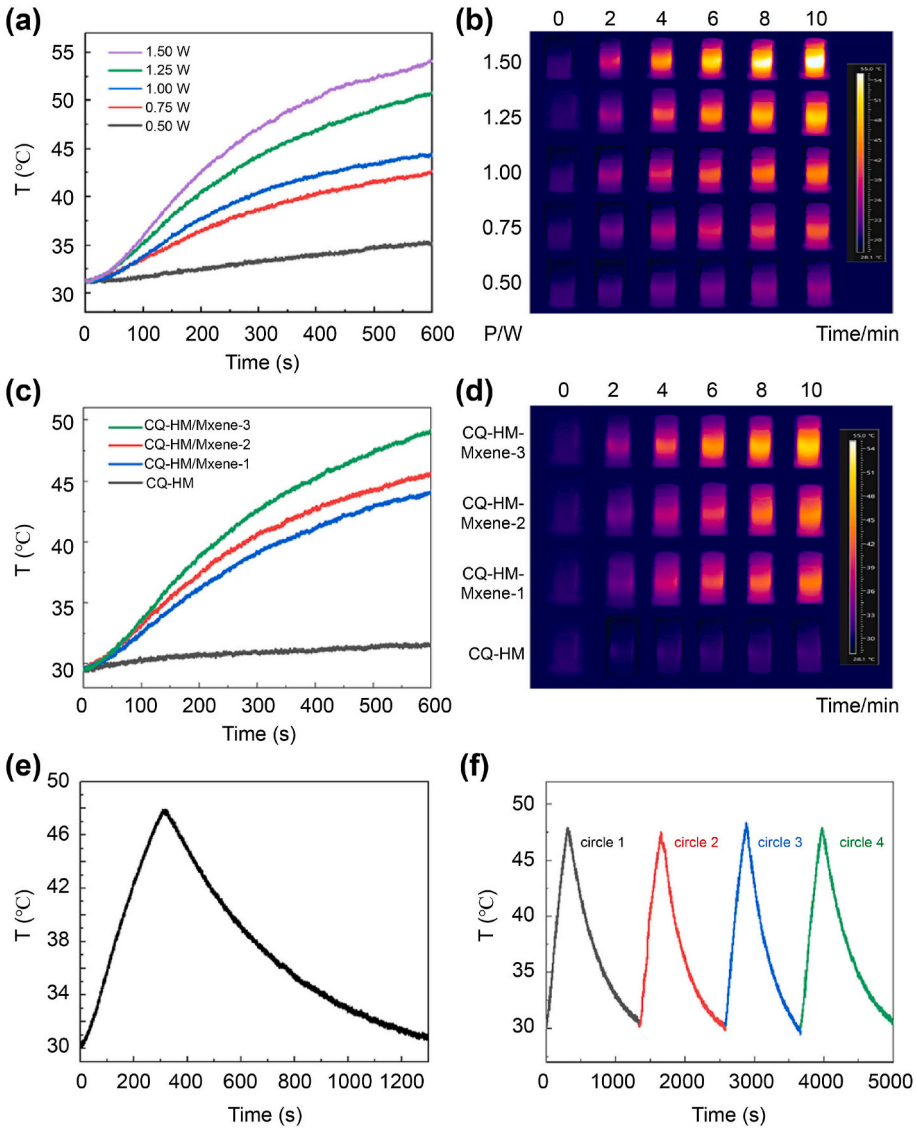

Fig. 4. (a) ~ (b) Temperature increase of the CQ-HM/MXene-1 hydrogel under NIR irradiation of 0.5, 0.75, 1.0, 1.25 and 1.5 W/cm^2 for 10 min. (c) ~ (d) Temperature increase profiles of the CQ-HM, CQ-HM/MXene-1, CQ-HM/MXene-2, and CQ-HM/MXene-3 hydrogels under NIR irradiation of 1.0 W/cm^2 for 10 min. (e) ~ (f) Temperature changes of the CQ-HM/MXene-3 hydrogel during five on/off cycles of NIR irradiation at 1.0 W/cm^2 for 100 min.

the medium in the experimental group was replaced with hydrogel, while the medium was used as the control group. Consequently, cell viability was assessed using the CCK-8 assay after 24 and 72 h. Simultaneously, a mixture of Calcein-AM (2 μmol/L $^{-1}$) and PI (4.5 μmol/L) was added to the culture medium to stain the cells in various states, and then the cell morphology was observed by fluorescence microscope (Fig. 5(a)). It was found that a large number of living cells were observed on the surface of the hydrogels. Throughout the culture procedure, all cells displayed extensive dispersion, showcasing the superior cell adhesion of CQ-HM, CQ-HM/MXene-1, CQ-HM/MXene-2, and CQ-HM/MXene-3 hydrogels. Quantitative cell viability was further assessed using the CCK-8 assay after 1 and 3 days of culture (Fig. 5(b)). The percentage of living cells in all the hydrogels reminded at 90 % (Fig. 5 (c)). These results suggest that all the hydrogels exhibited excellent biocompatibility properties to fibroblasts. The addition of MXene did not compromise their cytotoxicity, and they served as effective hydrogel substrates for enhancing cell proliferation (see Fig. 5).

2.7. Antimicrobial activity

Rapid bacterial growth is a major factor that hinders the healing process of infected wounds. Therefore, the development of antibacterial hydrogels is crucial for promoting wound healing. By incorporating Ti_3C_2 Mxene into the hydrogel, the antibacterial properties can be significantly enhanced due to the generation of high temperatures through the conversion of light. To evaluate the antibacterial properties of the hydrogels, the agar disc diffusion method was employed. The activity of the hydrogels was assessed against both Gram-positive bacteria, such as *Staphylococcus aureus* (*S. aureus*), and Gram-negative bacteria, such as *Escherichia coli* (*E. coli*). The hydrogels were cut into 1 cm diameter circles and placed in a 24-well plate. After sterilization through alcohol immersion, 1 mL of bacterial solution with a concentration of 1 × 10^7 CFU/mL was added to each agar disc. The antimicrobial activity of CQ-HM, CQ-HM/MXene-1, CQ-HM/MXene-2, and CQ-HM/MXene-3 hydrogels was evaluated through the following experiments: (1) The circular hydrogel was mixed with 1 mL of bacterial solution and incubated for 3 h with a rotation speed of 220 rpm. After gradient dilution, samples were plated on agar plates and the colony-

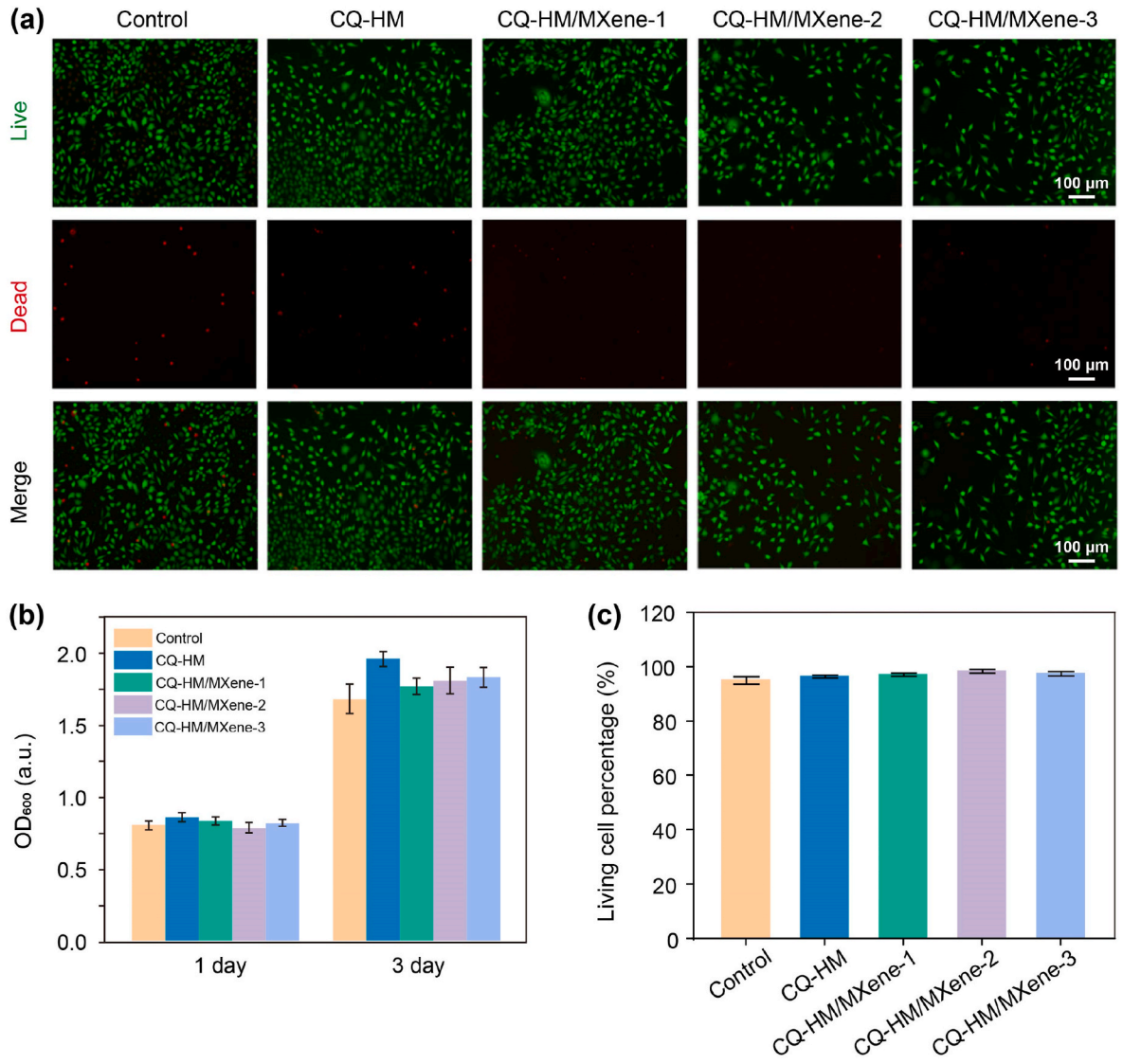

Fig. 5. (a) Images of L929 cultured on the PBS Control, CQ-HM, CQ-HM/MXene-1, CQ-HM/MXene-2, and CQ-HM/MXene-3 hydrogels for 48 h, where dead cells were stained red and live cells were stained green; (b) Cytotoxicity of different samples assessed by Cell Counting Kit-8 (CCK-8) assay for 1 and 3 days; (c) Percentage of living cells treated with different hydrogels observed by live/dead cell staining. (For interpretation of the references to colour in this figure legend, the reader is referred to the Web version of this article.)

forming units (CFUs) were counted; (2) The circular hydrogel was pre-treated with or without 808 nm NIR with a power of 1.0 W at a distance of 15 cm from the hydrogel for 10 min, and then 1 mL of bacterial solution was added for incubation. The control group without hydrogel addition also underwent the same test procedures and was cultured at 37 °C for 24 h before being counted. The anti-bacterial efficacy of the hydrogel was determined by calculating the mean value from five repetitions of each test group. The number of bacteria in the control group (treatment with PBS) remained unchanged with or without 808 nm NIR. The relative bacterial viability for the control group with or without NIR irradiation was 99 %. However, for CQ-HM, CQ-HM/MXene-1, CQ-HM/MXene-2, and CQ-HM/MXene-3 groups, the viability was nearly 70 % for both *E. coli* and *S. aureus* without NIR radiation due to the inherent antibacterial property of the quaternary ammonium salt on CQ. Simultaneously, the relative bacterial viability for CQ-HM, CQ-HM/MXene-1, CQ-HM/MXene-2, and CQ-HM/MXene-3 was 69.95 ± 1.89 %, 58.42 ± 1.07 %, 28.52 ± 0.54 %, and 3.07 ± 0.59 % respectively for *E. coli* (Fig. 6(c)) and 68.67 ± 1.79 %, 56.62 ± 2.07 %, 30.52 ± 0.64 %, and 1.56 ± 0.62 % for *S. aureus* (Fig. 6(d)) with 808 nm NIR light radiation. Compared to the control, CQ-HM showed slight antibacterial ability, while CQ-HM/MXene-1, CQ-HM/MXene-2, CQ-HM/MXene-3 demonstrated much higher antibacterial efficiency. CQ-HM/MXene-3 illustrated the most excellent antibacterial property due to the highest MXene content and best PTT effect (See Fig. 6).

2.8. *In vivo* wound healing

The CQ-HM, CQ-HM/MXene-1, CQ-HM/MXene-2, and CQ-HM/MXene-3 hydrogel was injected onto the round full-thickness wound of the SD mice and then irradiated with 395 nm light to form the hydrogels for infected wound therapy. In the case of an infected wound, the promotion of bacterial reproduction delayed the closure of the wound and increases the burden on healthcare providers. To assess the potential clinical application of CQ-HM/MXene hydrogels, a SD rat model with an infected wound was created. This model was used to investigate the infected of the hydrogels to heal infected wounds. To evaluate the promotion of wound healing properties of the hydrogels, the SD mice were divided into four groups: control group, CQ-HM, CQ-HM/MXene-1, CQ-HM/MXene-2, and CQ-HM/MXene-3 with the 808 nm NIR irradiation. In Fig. 7, the wound closure rate in the CQ-HM, CQ-HM/MXene-1, CQ-HM/MXene-2, CQ-HM/MXene-3 groups surpassed 50 % after 3 days of treatment with NIR irradiation. This healing rate

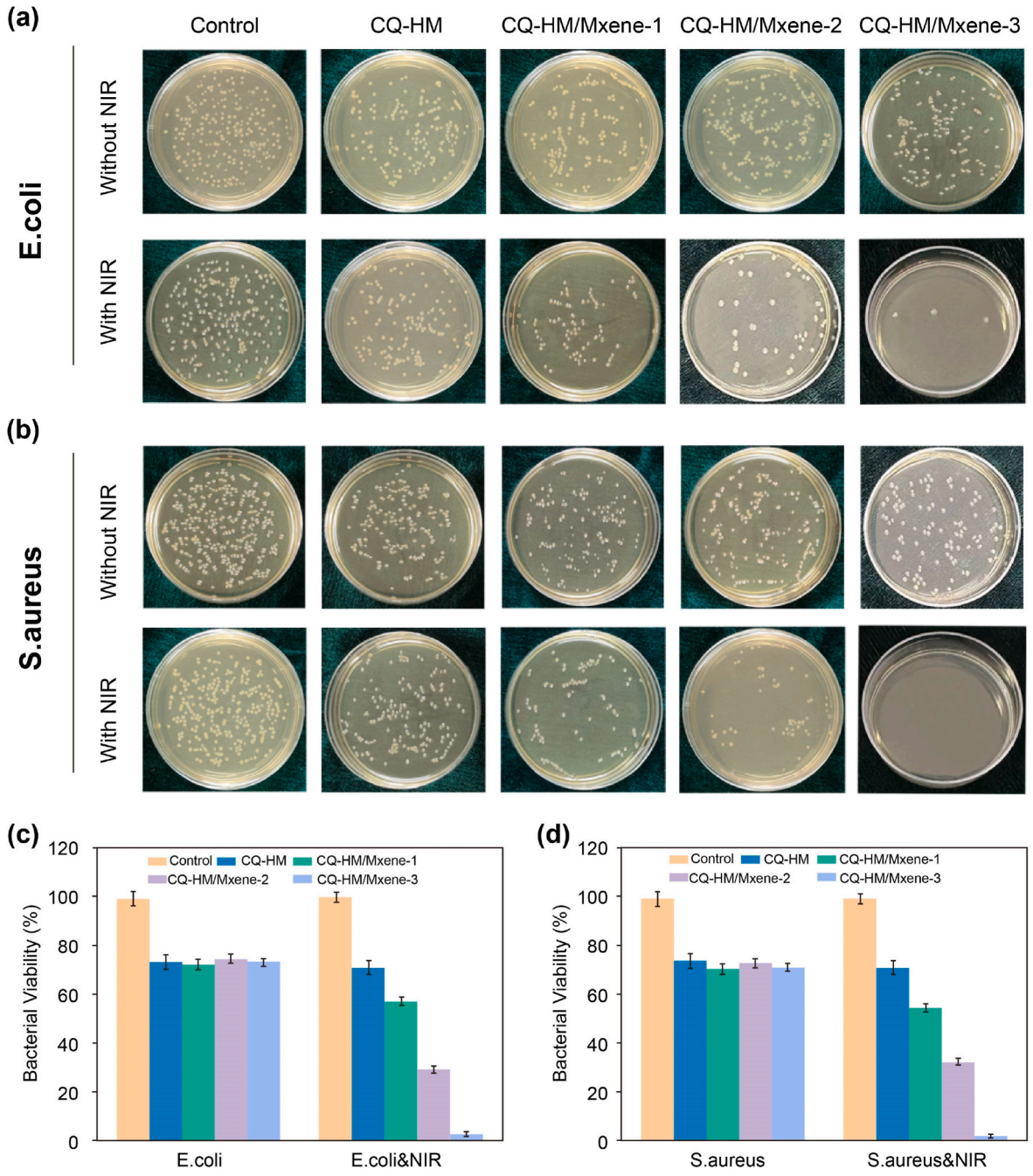

Fig. 6. Antimicrobial activity of the hydrogel treatments against *E. coli* (a) and *S. aureus* (b) as observed by colony forming units (CFU) after 24 h of co-incubation with the hydrogel. (c)~(d) Quantitative results of live/dead staining for *S. aureus* and *E. coli*.

exceeded that of the control and CQ-HM groups. After 10 days of treatment, with the protective layer formed by the irradiation of 395 nm UV light on the injectable hydrogel, the wounds treated with CQ-HM/MXene-1, CQ-HM/MXene-2, and CQ-HM/MXene-3 with 808 nm NIR light irradiation almost healed (Fig. 7(b)). However, in comparison, the control group and CQ-HM group exhibited only half the healing area of the wound, indicating that the hydrogel containing MXene demonstrated a strong bactericidal effect as a wound dressing due to its excellent photothermal properties. On the 10th day, the infected wounds treated with the CQ-HM/MXene-1, CQ-HM/MXene-2, and CQ-HM/MXene-3 groups, which were irradiated with 808 nm NIR, had an area of only 2.1 %, 1.2 % and 0.7 %, respectively. In contrast, the wound area treated with CQ-HM and the control group, both with 808 nm NIR irradiation was 18 % and 25 %, respectively (Fig. 7(b), (c), and (d)). This suggested that the skin condition of the mice in the former group had returned to normal. This result illustrated that the hydrogel with the photothermal material MXene could accelerate healing process for infected wounds. Finally, systemic toxicity was evaluated to ensure clinical safety clinical safety. Liver, spleen, heart, lung and kidney tissues were collected for all the groups. No obvious alterations were observed in these organs (Fig. 8), demonstrating that the biomaterials show no systemic toxicity and can be safely used as a wound dressing.

3. Discussion

3.1. The preparation of the CQ-HM/MXene hydrogels

As a wound dressing, the hydrogels should possess desirable softness,

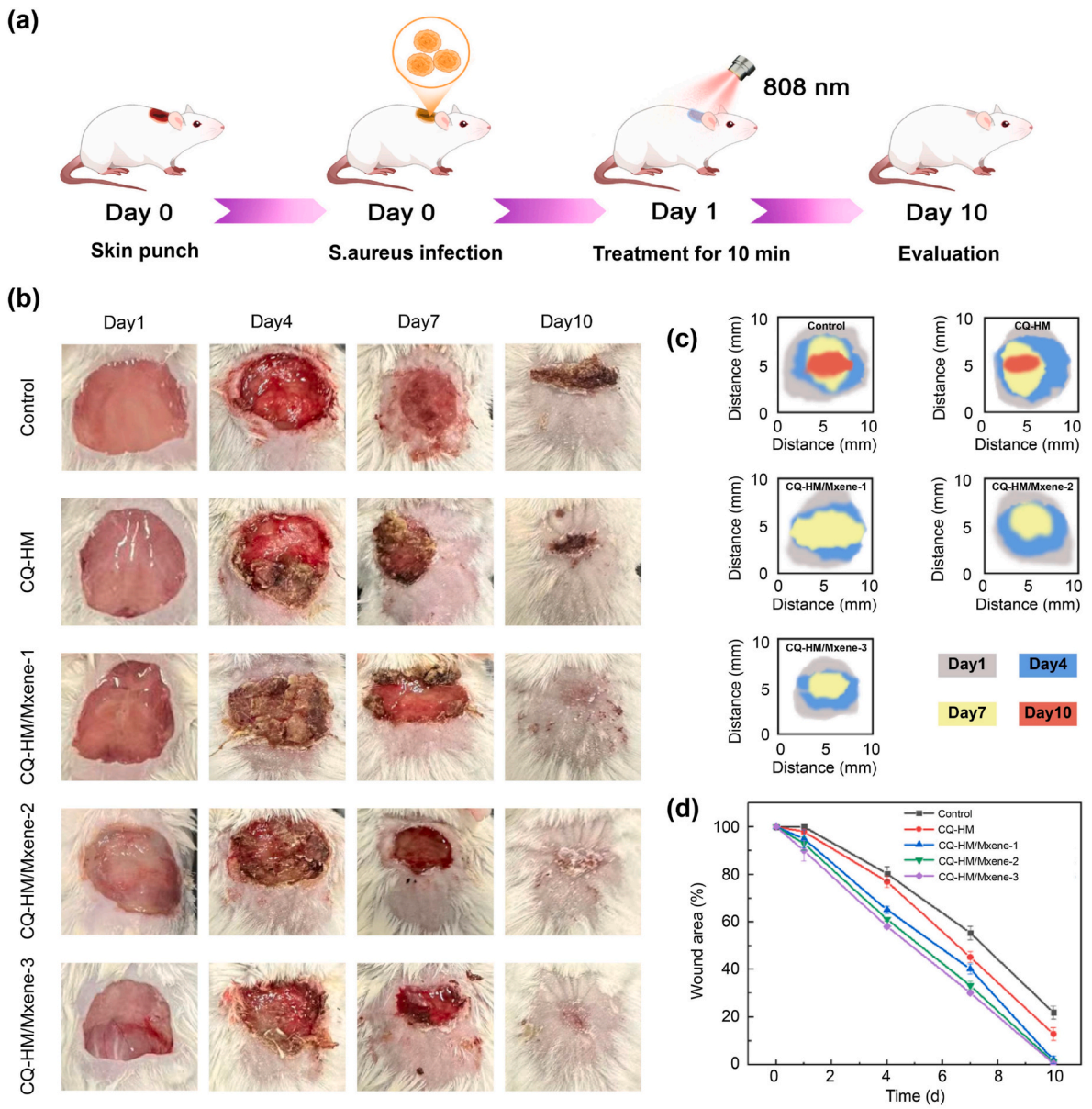

Fig. 7. (a) Infected diabetic wound model with PTT diagram in vivo; (b) Photographs of wounds with different treatments on days 1, 4, 7, and 10. (c) Traces of wound-bed closure on days 1, 4, 7, and 10 and (d) The time dependence of wound areas in the Control, CQ-HM, CQ-HM/MXene-1, CQ-HM/MXene-2, and CQ-HM/MXene-3 hydrogel groups with NIR irradiation.

injectable ability, swelling behaviors, and hydrophilicity. They should be injected to fit the wound with complex shapes and completely cover the irregular wound to prevent bacterial invasion. Chitosan, a natural polymer, after being grafted with 3-chloro-2-hydroxypropyl trimethyl ammonium chloride, showed enhanced antibacterial properties. Hyaluronic acid, another kind of biocompatible polymer, after being grafted with a methylacrylate group, can be cross linked by 395 nm UV light irradiation. Both ^{1}H NMR and FTIR illustrated the successful grafting of the polymers CQ and HM. Therefore, after being mixed with the photothermal material MXene, CQ and HM could form a 3D network structure antibacterial hydrogel after 395 nm UV light irradiation. The mapping images of SEM illustrated that Mxene is distributed homogeneously in the hydrogel, indicating that the hydrogel could transfer NIR light into heat energy. Simultaneously, the elevated fluid absorption capacity is advantageous for these CQ-HM/MXene hydrogels to be utilized in wound dressings, as it facilitates the maintenance of a moist microenvironment and the absorption of excessive wound exudates. The optimized storage modulus of the prepared hydrogels exhibited remarkable flexibility, allowing them to effectively conform to the wound site and replicate the characteristics of the natural tissue matrix.

3.2. *The photothermal effect of the CQ-HM/MXene hydrogels*

The CQ-HM/MXene hydrogel that was prepared exhibited a controlled photothermal transfer effect. It is crucial to have a mild PTT at a temperature below 50 °C for effectively treating bacterial infections in wound dressing. This is achieved by adjusting various experimental parameters, such as the concentration of photothermal materials, laser power density, and irradiation time. To mitigate any adverse effects resulting from uncontrolled heat generation, the MXene content in the hydrogel was adjusted to 1 mg/mL and the laser power density was set at 1.0 W, ensuring that it would not cause thermal damage to healthy tissues and organs.

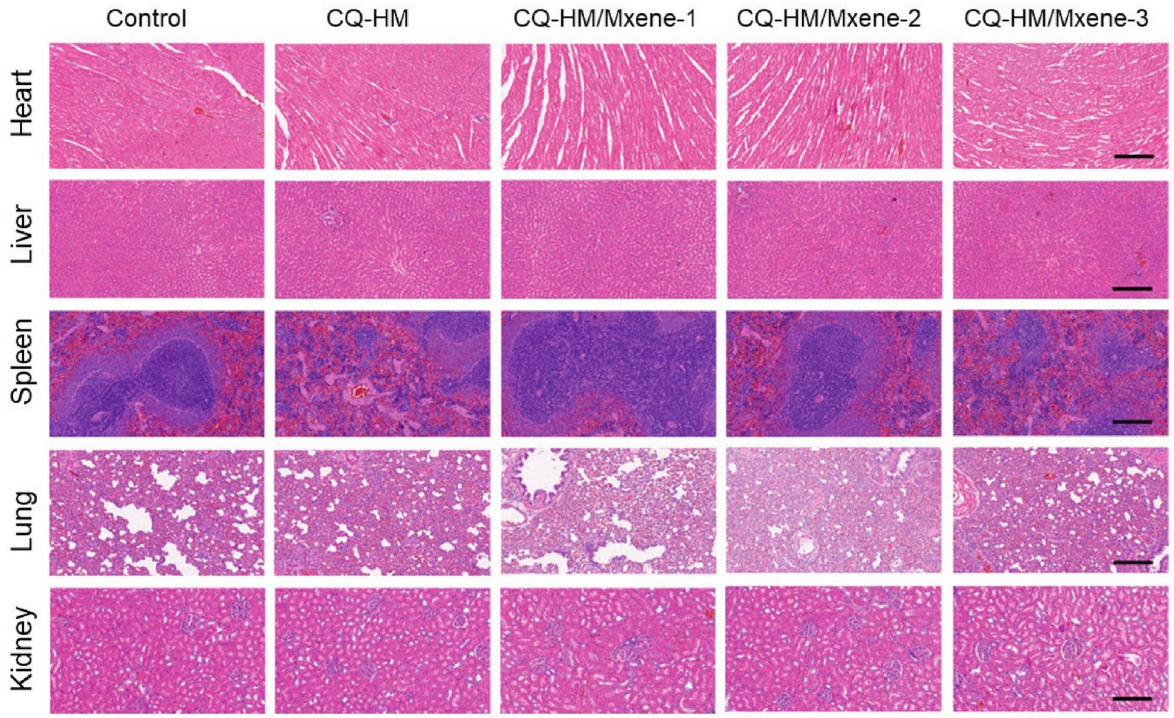

Fig. 8. Histological observations were made of the H&E-stained organs (heart, liver, spleen, lung, and kidney) in SD rats treated with control and different hydrogels (Scale bar, 200 μm).

3.3. The cytotoxicity, anti-bacteria and wound healing property of the CQ-HM/MXene hydrogels

Throughout the culture procedure, all cells displayed extensive dispersion, showcasing the superior cell adhesion of CQ-HM, CQ-HM/MXene-1, CQ-HM/MXene-2, and CQ-HM/MXene-3 hydrogels [35]. All of the hydrogels depicted excellent cell viability. As a biocompatible polymer, both CQ and HM illustrated low cytotoxicity. Simultaneously, these results suggest that the CQ-HM/MXene hydrogels exhibited excellent adhesion to fibroblast. The addition of MXene did not compromise their biocompatibility, and they served as effective hydrogel substrates for enhancing cell proliferation.

For infected wound healing, increasing the antibacterial effect is a vital point for the wound dressing. CQ grafted with 3-chloro-2-hydroxypropyl trimethyl ammonium chloride can provide some of the antibacterial function for the hydrogel. This can be attributed to the positively charged protonated ammonium (-NH_3^+) on the CQ, which can adsorb onto the surface of bacteria and form a layer of macromolecular film to prevent the delivery of nutrients to cells. This inhibits and kills bacteria [36]. Simultaneously, MXene demonstrated excellent photothermal properties, which can be used for anti-bacterial purposes due to the increase temperature when exposed to NIR irradiation at 808 nm. Under moderate conditions, the CQ-HM/MXene hydrogel is exceptionally bactericidal due to the synergistic effect of these two antibacterial properties. The number of bacteria in the control group (treatment with PBS) remained unchanged. After treatment with the hydrogels alone, the antibacterial properties of CQ reduced the number of bacteria, and the bacterial survival rate was 70 %. Although CQ-HM/MXene by itself possessed some antibacterial properties, they were insufficient for effective antibacterial activity. Therefore, the photothermal effect was added to the antibacterial system. By applying NIR, MXene in the hydrogel absorbed NIR energy and converted it into heat energy, thereby increasing the hydrogel's temperature to inhibit bacterial activity. The antibacterial rate of the CQ-HM/MXene hydrogel was up to 98 %.

Inspired by the promising in vitro antibacterial outcomes, an animal model with bacterial infections was created to assess the in vivo therapeutic benefits of the CQ-HM/MXene hydrogel. The CQ-HM/MXene hydrogel was applied at 49 °C to maintain antibacterial properties while minimizing thermal harm to neighboring healthy tissues and organs. A round skin wound was created on the back of each mouse, followed by the inoculation of *E. coli* and *S. aureus*. for bacterial infections. The presence of CQ-HM/MXene facilitated the close adhesion of the hydrogel to the wound due to the surface tension of water. In terms of wound healing, while all groups showed reduced infected areas over time, the CQ-HM/MXene-3 group exhibited the fastest recovery rate compared to the blank group. Simultaneously, the application of the hydrogel significantly promoted the healing of the infected wounds and showed no toxicity to the tissue.

4. Experimental and methods

4.1. Materials

Chitosan (with a degree of deacetylation of 80–95 % and a viscosity of 100–200 mPa s), acetic acid, sodium hydroxide, and methylacrylate were purchased from Sinopharm Chemical Reagent Co., Ltd. Glycidyl trimethylammonium chloride was acquired from Beijing InnoChem S cience & Technology Co., Ltd. Ti_3C_2 MXene was obtained from Shanghai Titan Scientific Co., Ltd., and Macklin Biochemical Co., Ltd., respectively. *Escherichia coli* (*E. coli*, BNCC 133264), *Staphylococcus aureus* (*S. aureus*, BNCC 186335) and methicillin-resistant staphylococcus aureus (MRSA, BNCC 330041) were obtained from BeNa Culture Collection (Henan, China). L929 cells were obtained from iCell Bioscience Inc (Shanghai, China). Endothelial cell culture medium (ECM), Dulbecco's Modified Eagle Medium (DMEM) and fetal bovine serum (FBS) were purchased from Sciencell Co., Ltd (USA). 0.5 % trypsin-ethylene diamine tetraacetic acid (EDTA) and penicillin-streptomycin were purchased from Gibico Co., Ltd (USA). The CCK-8 assay kit was purchased from Novozymes BioScience Co., Ltd (Nanjing, China). Mueller-Hinton Broth medium (MHB) and Lysogeny broth (LB) were purchased from Thermo Fisher Scientific Co., Ltd (USA). Other reagents

were utilized without further purification.

4.2. Preparation of CQ

CQ was synthesized according to the reference reported before [37]. Briefly, 2.5 g of chitosan was dissolved in 200 mL of 0.5 % (v/v) acetic acid with stirring. Then, 1546 μL of glycidyl trimethylammonium chloride was added drop wise to the chitosan solution and stirred vigorously at 55 °C for 24 h. After the reaction, the precipitate was filtered and the solution was dialyzed in deionized water for 72 h to remove impurities. Finally, the dialysate was freeze-dried to obtain the white powder CQ.

4.3. Preparation of HM

HM was synthesized according to reference [34]. Briefly, 2.5 g of hyaluronic acid was dissolved in 200 mL of deionized water, and then 2.0 mL of methylacrylate was added dropwise into the hyaluronic acid solution and stirred vigorously at 50 °C for 24 h. After the reaction, the reaction solution was dialyzed in deionized water for 72 h to remove impurities. Finally, the dialysate was freeze-dried to obtain the white powder HM.

4.4. Characterization of the polymer CQ and HM

The prepared *CQ* and *HM* polymer was characterized with ^{1}H NMR and FTIR spectra to confirm the successful grafting of glycidyl trimethylammonium chloride and methylacrylate. First, CQ and HM were characterized by ^{1}H NMR with the solvent $CDCl_3$, using trimethylsilane as the internal standard with 120 scans. An FTIR spectrometer (Nicolet iS 10, Thermo Fisher Scientific) was used to detect the FTIR spectra of CS, CQ, HA and HM. The FTIR wavenumber range was from 4000 to 1000 cm^{-1}.

4.5. Fabrication of the photothermal hydrogels

To prepare the photothermal hydrogel CQ-HM/Mxene, the CQ-HM solutions were obtained by dissolving CQ and HM in DI water. Then, different amounts of Mxene were mixed in 4 mL of CQ-HM aqueous solution with MXene concentrations of 0 mg/mL, 1 mg/mL, 2 mg/mL, and 3 mg/mL for half an hour at room temperature. Subsequently, 5 μL of a LAP solution was added to the above mixture and stirred vigorously for 10 min in the dark. The mixture was then extracted with a syringe and injected into molds. Finally, molds of different shapes were filled with the mixture and irradiated with 395 nm UV light for 5 s to form the hydrogels. The resulting photothermal hydrogels prepared above are labeled as CQ-HM, CQ-HM/Mxene-1, CQ-HM/Mxene-2, CQ-HM/Mxene-3 hydrogels, respectively.

4.6. Scanning electron microscope (SEM) measurement of the hydrogels

The hydrogel samples were freeze-dried before measurement, and then cut into small pieces. The cross section was pasted on a metal stage, and sputtered with gold powder. The microstructure of the hydrogel samples was detected using a SEM (SU1510, Hitachi Co. Ltd., Tokyo, Japan). The pore diameters of the samples were measured with Image J.

4.7. Swelling behaviors

The swelling ratios of the samples were evaluated via the immersion method with PBS at ambient temperature. The cylindrical hydrogel samples (diameter of 8 mm and height of 5 mm) were weighed. After immersion for different time intervals, the weights of the hydrogels were measured. The swelling ratios of hydrogels were defined by the following formula:

$$W\% = \frac{W_t - W_0}{W_0} \times 100\%$$

where W_0 represents the initial weight of the hydrogel and W_t represents the weight of the hydrogel after immersion in PBS. Each group of samples was measured at least five times and expressed as the mean and standard deviation.

4.8. Rheological properties

The rheological properties of the hydrogels were determined by a rheometer (Anton Paar rheometer, Austria). The sol precursor of the CQ-HM/Mxene was injected into the mold and shaped as discs with a diameter of 25 mm and a thickness of 1 mm by exposing it to 395 nm UV light for 5 s. For the hydrogel frequency scanning tests, the strain amplitude at 1 % once the gel stabilizes, and adjust angular frequency was adjusted within the range of 0.1–100 rad/s. For the strain scanning tests, the frequency amplitude was kept at 1 rad/s after stabilization, and the strain was adjusted within the range of 0.1–200 %

4.9. Photothermal properties of hydrogel

To evaluate the photothermal properties, the CQ-HM/Mxene hydrogels were irradiated with an 808 nm laser at different electrical powers (0 W/cm^2, 0.5 W/cm^2, 0.75 W/cm^2, 1.0 W/cm^2, 1.25 W/cm^2 and 1.5 W/cm^2). The CQ-HM, CQ-HM/MXene-1, CQ-HM/MXene-2, and CQ-HM/MXene-3 hydrogels were also irradiated separately. Deionized water was used as the control group. The temperature change of the CQ-HM/Mxene hydrogels was recorded using an infrared thermal imager. To detect the heating-cooling recycle photothermal properties of the hydrogels, the CQ-HM/MXene hydrogels were irradiated with an 808 nm laser (1.0 W/cm^2) for 10 min and then cooled to room temperature. The temperature change was recorded using an infrared thermal imager. This process was repeated 5 times to certify the photothermal stability of the CQ-HM/MXene hydrogels.

4.10. Cytotoxicity and photothermal toxicity in vitro

4.10.1. Cell culture

L929 cells were cultured in high glucose DMEM with 10 % FBS, 1 % penicillin and streptomycin. The cell was incubated under standard culture conditions of 37 °C, 5 % CO_2 and 95 % air.

4.10.2. CCK-8 assay

To assess the toxicity of the hydrogel, L929 cells were seeded onto the surfaces of TCP, CQ-HM, CQ-HM/Mxene-1, CQ-HM/Mxene-2, and CQ-HM/Mxene-3 hydrogels at a density of 5.0×10^4 per sample. Subsequently, L929 in each group were exposed to NIR laser (808 nm, 1.0 W/cm^2) for 10 min and then incubated at 37 °C for 24 and 72 h. Cell viability was evaluated using a CCK-8 assay. Then, 10 μL of CCK-8 solution was added to each well and incubated at 37 °C for 2 h. The absorbance at 450 nm was measured using an enzyme-labeling instrument (357–808025, Thermo Fisher Scientific Inc, China).

4.10.3. Cell live/dead assay

The Live/Dead assay was carried out to analyze the cell proliferation of the hydrogels. L929 cells were cultured on different groups of hydrogels. After 24 h of incubation under an NIR laser (808 nm, 1.0 W/cm^2, 10 min), the cells were stained with Calcein-AM/PI for 30 min at 37 °C. Images were obtained by confocal microscopy (TCS SP8, Leica, Wetzlar, Hesse, Germany). Calcein-AM/PI was used to mark living and dead cells, respectively. The ratio of the number of dead or live cells was analyzed in three random fields.

4.11. Antibacterial activity and photothermal antibacterial effect measurements in vitro

In order to assess the antibacterial efficacy of the hydrogels, *S. aureus* and *E. coli* were chosen as representative strains of Gram-positive and Gram-negative bacteria, respectively. Bacterial cells were cultured in Muller-Hinton broth medium (MHB) at 37 °C with agitation at 120 rpm, followed by uniform dispersion in PBS at a colony forming unit (CFU) concentration of around 10^6 mL^{-1}. 1 mL of bacterial suspension was then added to the buffer coated with PBS control, CQ-HM, CQ-HM/Mxene-1, CQ-HM/Mxene-2, CQ-HM/Mxene-3, respectively, and incubated at 37 °C for 12 h before being irradiated with an NIR laser (808 nm, 1.0 W/cm^2, 10 min).

4.11.1. Plate coating assay

Bacterial suspensions were adjusted to a concentration of 10^3 CFU mL^{-1}, and aliquots were spread onto lysogeny broth (LB) agar plates. After incubation at 37 °C for 12 h, images of the bacterial plates were captured and analyzed using ImageJ software to assess the antibacterial efficacy of various samples.

4.12. In vivo antibacterial and wound healing promotion

All animal experiments were approved by the Animal Ethics Committee of SiPeiFu (Beijing) Biotechnology Co., Ltd., and were carried out under the Guidelines for the Care and Use of Animals at SiPeiFu (Beijing) Biotechnology Co., Ltd. (The Ethical Clearance number is 2022030101). Male SD rats with an average body weight of 250 ± 30 g were used for full-thickness wound healing experiments.

The wound healing properties of CQ-HM/Mxene hydrogel were tested in vivo using adult SD rats. The skin of the rats was excised by total dermal excision to form a circular wound of approximately 1 cm in diameter, and the wound was injected with $1*10^5$ methicillin-resistant *S.aureus*. The constructs were modeled on infected wounds. SD rats were randomly divided into the following five groups (n = 5): (1) PBS; (2) CQ-HM; (3) CQ-HM/Mxene-1; (4) CQ-HM/Mxene-2; (5) CQ-HM//Mxene-3. PBS was the control group. All gel groups were irradiated with 808 nm 1.0 W cm^{-2} NIR laser for 10 min. The different hydrogel treatments of the wounds were recorded on days 0, 1, 4, 7, and 10.

SD rats were euthanized on the 10th day after the indicated surgery. At the same time, major organs (heart, liver, spleen, lungs, and kidneys) were excised for hematoxylin and eosin (H&E) staining to study the potential toxicity of the gel on each group.

4.13. Statistical analysis

All of the data are denoted as means and standard deviations, and at least three tests were performed unless otherwise specified.

5. Conclusions

In this study, we developed and synthesized a novel biocompatible polymer-based antibacterial hydrogel for effective treatment of bacterial infections and wound healing. The hybrid polymer HM was synthesized by grafting MA onto the pendent segment of HA, while CS was modified with glycidyl trimethylammonium chloride to form CQ. These polymers were then combined with the 2D material MXene and cross-linked with the photoinitiator, LAP, under 395 nm UV light. The antibacterial and wound healing properties of the hydrogel could be adjusted by varying the amount of MXene added. The CQ-HM/MXene hydrogel exhibited a NIR photoexcitation response when exposed to NIR irradiation, attributed to the photothermal properties of MXene. The CQ-HM/MXene hydrogel demonstrated excellent antibacterial efficacy and low cytotoxicity, making it suitable for infected wound healing. This hydrogel demonstrated more competitiveness as an ideal dressing for promoting wound healing.

CRediT authorship contribution statement

Xinbo Ma: Writing – original draft, Project administration, Methodology, Investigation, Data curation. **Aoao Wang:** Formal analysis. **Xuelian Zhang:** Project administration. **Juan Zhang:** Formal analysis. **Jiawei Li:** Formal analysis. **Xi Fu:** Writing – original draft, Methodology. **Peng Wang:** Writing – review & editing. **Yantao Zhao:** Writing – review & editing, Methodology. **Xiaonan Huang:** Writing – review & editing, Supervision, Methodology, Funding acquisition, Conceptualization.

Declaration of competing interest

The authors declare that they have no known competing financial interests or personal relationships that could have appeared to influence the work reported in this paper.

Data availability

The data that has been used is confidential.

Acknowledgments

This work was funded by the National Natural Science Foundation of China (82151312, 82272493 and 52172249), the Beijing Science Nova Program (20220484155), the Haidian Frontier Project of the Beijing Natural Science Foundation (No. L212067), and the Capital Clinical Diagnosis and Treatment Technology Research and Transformation Application Project (Z201100005520060).

References

[1] S. Zhang, T. Jiang, F. Han, L. Cao, M. Li, Z. Ge, H. Sun, H. Wu, W. Wu, N. Zhou, M. L. Akhtar, H. Jiang, A wearable self-powered microneedle system based on conductive drugs for infected wound healing: a new electrical stimulation delivery strategy, Chem. Eng. J. (Amsterdam, Neth.) 480 (2024) 148347, https://doi.org/10.1016/j.cej.2023.148347.

[2] R. Zhang, X. Huang, Q. Wu, S. Chu, X. Bai, Y. Zhou, J. You, C. Yang, H. Tan, Multifunctional gelatin nanoparticle stabilized-pickering emulsion hydrogel based on dextran and amikacin with controlled drug release and enhanced antibacterial capability for promoting infected wound healing, Int. J. Biol. Macromol. 262 (2024) 130172, https://doi.org/10.1016/j.ijbiomac.2024.130172.

[3] X. Zhai, H. Hu, M. Hu, S. Ji, T. Lei, X. Wang, Z. Zhu, W. Dong, C. Teng, W. Wei, A nano-composite hyaluronic acid-based hydrogel efficiently antibacterial and scavenges ROS for promoting infected diabetic wound healing, Carbohydr. Polym. 334 (2024) 122064, https://doi.org/10.1016/j.carbpol.2024.122064.

[4] P. Yang, Y. Ju, X. Liu, Z. Li, H. Liu, M. Yang, X. Chen, L. Lei, B. Fang, Natural self-healing injectable hydrogels loaded with exosomes and berberine for infected wound healing, Mater. Today Bio. 23 (2023) 100875, https://doi.org/10.1016/j.mtbio.2023.100875.

[5] J. Yang, H. Yu, L. Wang, X. Liu, Y. Huang, Y. Hong, S. Ren, Mussel-inspired near-infrared light-responsive gelatin-based hydrogels for enhancing MRSA-infected wound healing, Int. J. Biol. Macromol. 263 (2024) 129887, https://doi.org/10.1016/j.ijbiomac.2024.129887.

[6] S. Wu, L. Zhu, S. Ni, Y. Zhong, K. Qu, X. Qin, K. Zhang, G. Wang, D. Sun, W. Deng, W. Wu, Hyaluronic acid-decorated curcumin-based coordination nanomedicine for enhancing the infected diabetic wound healing, Int. J. Biol. Macromol. 263 (2024) 130249, https://doi.org/10.1016/j.ijbiomac.2024.130249.

[7] W. Wang, B. Jia, H. Xu, Z. Li, L. Qiao, Y. Zhao, H. Huang, X. Zhao, B. Guo, Multiple bonds crosslinked antibacterial, conductive and antioxidant hydrogel adhesives with high stretchability and rapid self-healing for MRSA infected motion skin wound healing, Chem. Eng. J. (Amsterdam, Neth.) 468 (2023) 143362, https://doi.org/10.1016/j.cej.2023.143362.

[8] M. Wang, W. Zhang, C. Wang, L. Xiao, L. Yu, J. Fan, Hemostatic and antibacterial calcium–copper zeolite gauze for infected wound healing, RSC Adv. 14 (2024) 878–888, https://doi.org/10.1039/D3RA06070E.

[9] K. Wang, H. Wang, Y. Liu, Z. Li, Metal-ion Co-doped nanofilm with anti-bacterial and pro-angiogenic activities to accelerate infected wound healing, Mater. Today Commun. 36 (2023) 106870, https://doi.org/10.1016/j.mtcomm.2023.106870.

[10] J. Wang, X. Ge, Y. Xiang, X. Qi, Y. Li, H. Xu, E. Cai, C. Zhang, Y. Lan, X. Chen, Y. Shi, Z. Li, J. Shen, An ionic liquid functionalized sericin hydrogel for drug-resistant bacteria-infected diabetic wound healing, Chin. Chem. Lett. (2024) 109819, https://doi.org/10.1016/j.cclet.2024.109819.

[11] J. Teng, W. Zhao, S. Zhang, D. Yang, Y. Liu, R. Huang, Y. Ma, L. Jiang, H. Wei, J. Zhang, J. Chen, Injectable nanoparticle-crosslinked xyloglucan/ε-poly-l-lysine composite hydrogel with hemostatic, antimicrobial, and angiogenic properties for

infected wound healing, Carbohydr. Polym. (2024) 122102, https://doi.org/10.1016/j.carbpol.2024.122102.
[12] W. Song, D. Wang, S. Xiao, X. He, W. Xiong, J. Shen, NIR-II-Amplify high-entropy MXene-based sonosensitizer as sonodynamic therapy promotes methicillin-resistant Staphylococcus aureus–infected wound healing, Mater. Des. 240 (2024) 112857, https://doi.org/10.1016/j.matdes.2024.112857.
[13] G. Shu, D. Xu, S. Xie, L. Chang, X. Liu, J. Yang, Y. Li, X. Wang, The antioxidant, antibacterial, and infected wound healing effects of ZnO quantum dots-chitosan biocomposite, Appl. Surf. Sci. 611 (2023) 155727, https://doi.org/10.1016/j.apsusc.2022.155727.
[14] X. Ren, L. Chang, Y. Hu, X. Zhao, S. Xu, Z. Liang, X. Mei, Z. Chen, Au@MOFs used as peroxidase-like catalytic nanozyme for bacterial infected wound healing through bacterial membranes disruption and protein leakage promotion, Mater. Des. 229 (2023) 111890, https://doi.org/10.1016/j.matdes.2023.111890.
[15] X. Qiu, L. Nie, P. Liu, X. Xiong, F. Chen, X. Liu, P. Bu, B. Zhou, M. Tan, F. Zhan, X. Xiao, Q. Feng, K. Cai, From hemostasis to proliferation: accelerating the infected wound healing through a comprehensive repair strategy based on GA/OKGM hydrogel loaded with MXene@TiO_2 nanosheets, Biomaterials 308 (2024) 122548, https://doi.org/10.1016/j.biomaterials.2024.122548.
[16] Y. Ouyang, X. Su, X. Zheng, L. Zhang, Z. Chen, Q. Yan, Q. Qian, J. Zhao, P. Li, S. Wang, Mussel-inspired "all-in-one" sodium alginate/carboxymethyl chitosan hydrogel patch promotes healing of infected wound, Int. J. Biol. Macromol. 261 (2024) 129828, https://doi.org/10.1016/j.ijbiomac.2024.129828.
[17] W. Luo, Y. Jiang, J. Liu, M. Ju, S. Algharib, A. Dawood, On-demand release of enrofloxacin-loaded chitosan oligosaccharide-oxidized hyaluronic acid composite nanogels for infected wound healing, Int. J. Biol. Macromol. 253 (2023) 127248, https://doi.org/10.1016/j.ijbiomac.2023.127248.
[18] X. Liu, Y. Sun, J. Wang, Y. Kang, Z. Wang, W. Cao, J. Ye, C. Gao, A tough, antibacterial and antioxidant hydrogel dressing accelerates wound healing and suppresses hypertrophic scar formation in infected wounds, Bioact. Mater. 34 (2024) 269–281, https://doi.org/10.1016/j.bioactmat.2023.12.019.
[19] N. Liu, S. Zhu, Y. Deng, M. Xie, M. Zhao, T. Sun, C. Yu, Y. Zhong, R. Guo, K. Cheng, D. Chang, P. Zhu, Construction of multifunctional hydrogel with metal-polyphenol capsules for infected full-thickness skin wound healing, Bioact. Mater. 24 (2023) 69–80, https://doi.org/10.1016/j.bioactmat.2022.12.009.
[20] K. Liu, D. Zhao, H. Zhao, Y. Yu, M. Yang, M. Ma, C. Zhang, F. Guan, M. Yao, Mild hyperthermia-assisted chitosan hydrogel with photothermal antibacterial property and CAT-like activity for infected wound healing, Int. J. Biol. Macromol. 254 (2024) 128027, https://doi.org/10.1016/j.ijbiomac.2023.128027.
[21] K. Liu, Y. Yu, H. Zhao, M. Yang, C. Zhang, F. Guan, M. Yao, Cowberry extract loaded chitosan hydrogel with photothermal and antioxidant properties promotes infected wound healing, Int. J. Biol. Macromol. 262 (2024) 129988, https://doi.org/10.1016/j.ijbiomac.2024.129988.
[22] Z. Li, D. Xu, Z. Deng, J. Yin, Y. Qian, J. Hou, X. Ding, J. Shen, X. He, Single-atom-catalyzed MXene-based nanoplatform with photo-enhanced peroxidase-like activity nanotherapeutics for staphylococcus aureus infection, Chem. Eng. J. (Amsterdam, Neth.) 452 (2023) 139587, https://doi.org/10.1016/j.cej.2022.139587.
[23] X. He, Y. Lv, Y. Lin, H. Yu, Y. Zhang, Y. Tong, C. Zhang, Platinum nanoparticles regulated V2C MXene nanoplatforms with NIR-II enhanced nanozyme effect for photothermal and chemodynamic anti-infective therapy, Adv. Mater. 36 (2024) 2400366, https://doi.org/10.1002/adma.202400366.
[24] X. He, J. Hou, X. Sun, P. Jangili, J. An, Y. Qian, J. Kim, J. Shen, NIR-II photo-amplified sonodynamic therapy using sodium molybdenum bronze nanoplatform against subcutaneous Staphylococcus aureus infection, Adv. Funct. Mater. 32 (2022) 2203964, https://doi.org/10.1002/adfm.202203964.
[25] Z. Li, M. Pan, Y. Yu, L. Bao, L. Yang, Y. Song, M. Wang, L. Si, X. Yu, M. Jiang, L. Xu, Polymer nanoparticles crosslinked by polyethyleneimine and hydroquinone with the selective antibacterial, antibiofilm and antioxidative activity to promote infected wound healing, Sustainable Mater. Technol. 39 (2024) e00817, https://doi.org/10.1016/j.susmat.2023.e00817.
[26] Y. Li, H. Li, Z. Yu, J. Liu, Y. Lin, J. Xu, C. Zhang, Q. Chen, X. Han, Q. Peng, Drug-free and multifunctional sodium bicarbonate/hyaluronic acid hybrid dressing for synergistic healing of infected wounds, Int. J. Biol. Macromol. 259 (2024) 129254, https://doi.org/10.1016/j.ijbiomac.2024.129254.
[27] W. Li, H. Su, Y. Ma, H. Ren, Z. Feng, Y. Wang, Y. Qiu, H. Wang, H. Wang, Q. Chen, Z. Zhu, Multicargo-loaded inverse opal gelatin hydrogel microparticles for promoting bacteria-infected wound healing, Int. J. Biol. Macromol. 260 (2024) 129557, https://doi.org/10.1016/j.ijbiomac.2024.129557.
[28] L. Li, Y. Wang, Z. Huang, Z. Xu, R. Cao, J. Li, B. Wu, J.R. Lu, H. Zhu, An additive-free multifunctional β-glucan-peptide hydrogel participates in the whole process of bacterial-infected wound healing, J. Controlled Release 362 (2023) 577–590, https://doi.org/10.1016/j.jconrel.2023.09.010.
[29] J. Li, Q. Ding, Y. Zha, J. Xie, F. Li, R. Li, N. Ao, The silk fibroin nanofibrous membrane loaded with polyhexamethyl biguanide for promoting infected wound healing, Eur. Polym. J. 202 (2024) 112666, https://doi.org/10.1016/j.eurpolymj.2023.112666.
[30] W. Guo, Y. Li, C. Zhu, Z. Duan, R. Fu, D. Fan, Tannic acid-Fe^{3+} dual catalysis induced rapid polymerization of injectable poly (lysine) hydrogel for infected wound healing, Int. J. Biol. Macromol. 249 (2023) 125911, https://doi.org/10.1016/j.ijbiomac.2023.125911.
[31] M. Cheng, L, G. Hu, P. Xu, Q. Pan, Z. Liu, Z. Zhang, C. He, M. Wang, L. Liu, J. Chen, Chen, tannic acid-based dual-network homogeneous hydrogel with antimicrobial and pro-healing properties for infected wound healing, Colloids Surf., B 227 (2023) 113354, https://doi.org/10.1016/j.colsurfb.2023.113354.
[32] Q. Chen, Zr, S. Yang, S. Du, L. Chen, J. Zhang, Zhu, polyphenol-sodium alginate supramolecular injectable hydrogel with antibacterial and anti-inflammatory capabilities for infected wound healing, Int. J. Biol. Macromol. 257 (2024) 128636, https://doi.org/10.1016/j.ijbiomac.2023.128636.
[33] Q. Ding, Z. Mo, X. Wang, M. Chen, F. Zhou, Z. Liu, Y. Long, X. Xia, P. Zhao, The antibacterial and hemostatic curdlan hydrogel–loading epigallocatechin gallate for facilitating the infected wound healing, Int. J. Biol. Macromol. 266 (2024) 131257, https://doi.org/10.1016/j.ijbiomac.2024.131257.
[34] H. Li, Y. Yang, M. Mu, C. Feng, D. Chuan, Y. Ren, X. Wang, R. Fan, J. Yan, G. Guo, MXene-based polysaccharide aerogel with multifunctional enduring antimicrobial effects for infected wound healing, Int. J. Biol. Macromol. 261 (2024) 1292388, https://doi.org/10.1016/j.ijbiomac.2024.129238.
[35] Z. Jia, D. Lin, C. Tang, X. Sun, L. Cao, L. Liu, Zinc-loaded human serum albumin methacryloyl microspheres with growth factors release for infected wound healing, Mater. Des. 239 (2024) 112810, https://doi.org/10.1016/j.matdes.2024.112810.
[36] X. Jiang, L. Yuan, P. Ming, M. Jiang, Y. Guo, S. Li, Y. Liu, C. Zhang, Z. Rao, J. Chen, Y. He, R. Cai, Z. Rao, J. Chen, Muscle-inspired lamellar chitosan sponge with photothermal antibacterial and antioxidant properties for hemostasis and accelerated bacteria infected wound healing, Appl. Mater. Today 35 (2023) 101992, https://doi.org/10.1016/j.apmt.2023.101992.
[37] F. Jiang, Y. Duan, Q. Li, X. Li, Y. Li, Y. Wang, S. Liu, M. Liu, C. Zhang, X. Pan, Insect chitosan/pullulan/gallium photo-crosslinking hydrogels with multiple bioactivities promote MRSA-infected wound healing, Carbohydr. Polym. 334 (2024) 122045, https://doi.org/10.1016/j.carbpol.2024.122045.